# Acousto-optical coherence tomography using random phase jumps on ultrasound and light

**M. Lesaffre[1,2], S. Farahi[1], M. Gross[2], P. Delaye[3], A.C. Boccara[1] and F. Ramaz[1]**

[1]*Institut Langevin, ESPCI ParisTech, CNRS UMR 7587, Laboratoire d'Optique Physique, 10 rue Vauquelin F-75231 Paris Cedex 05.*

[2]*Laboratoire Kastler-Brossel, UMR 8552 (ENS, CNRS, UMPC), Ecole Normale Supérieure, 10 rue Lhomond F-75231 Paris cedex 05*

[3]*Laboratoire Charles Fabry de l'Institut d'Optique, UMR 8501 (Institut d'Optique, CNRS, Univeristé Paris-Sud), Campus Polytechnique, RD 128, 91127 Palaiseau Cedex*

**Abstract:** Imaging objects embedded within highly scattering media by coupling light and ultrasounds (US) is a challenging approach. In deed, US enable direct access to the spatial localization, though resolution can be poor along their axis (cm). Up to now, several configurations have been studied, giving a millimetric axial resolution by applying to the US a microsecond pulse regime, as is the case with conventional echography. We introduce a new approach called Acousto-Optical Coherence Tomography (AOCT), enabling us to get a millimetric resolution with continuous US and light beams by applying random phase jumps on US and light. An experimental demonstration is performed with a self-adaptive holographic setup containing a photorefractive GaAs bulk crystal and a single large area photodetector.



**OCIS codes:** ocis: (170.1650) Coherence imaging, (170.3660) Light propagation in tissues, (290.7050) Turbid media, (090.0090) Holography, (090.2880) Holographic interferometry, (170.7050) Turbid media

## References and links

1. W. Leutz, and G. Maret, "Ultrasonic modulation of multiply scattered light," Phys. B: Phys. Condensed Matter **204**(1-4), 14–19 (1995).
2. L. Wang, S. L. Jacques, and X. Zhao, "Continuous-wave ultrasonic modulation of scattered laser light to image objects in turbid media," Opt. Lett. **20**(6), 629–631 (1995).
3. M. Kempe, M. Larionov, D. Zaslavsky, and A. Z. Genack, "Acousto-optic tomography with multiply scattered light", J. Opt. Soc. Am. A , **14**(5), 1151–1158 (1997).
4. S. Leveque, A. C. Boccara, M. Lebec, and H. Saint-Jalmes, "Ultrasonic tagging of photon paths in scattering media: parallel speckle modulation processing," Opt. Lett. **24**(3), 181–183 (1999).
5. A. Lev, and B. Sfez, "In vivo demonstration of the ultrasound-modulated light technique," J. Opt. Soc. Am. A **20**(12), 2347–2354 (2003).
6. A. Lev, and B. G. Sfez, "Pulsed ultrasound-modulated light tomography," Opt. Lett. **28**(17), 1549–1551 (2003).
7. A. Lev, E. Rubanov, B. Sfez, S. Shany, and A. J. Foldes, "Ultrasound-modulated light tomography assessment of osteoporosis," Opt. Lett. **30**(13), 1692–1694 (2005).
8. M. Gross, P. Goy, and M. Al-Koussa, "Shot-noise detection of ultrasound-tagged photons in ultrasound-modulated optical imaging," Opt. Lett. **28**(24), 2482–2484 (2003).
9. F. Le Clerc, M. Gross, and L. Collot, "Synthetic-aperture experiment in the visible with on-axis digital heterodyne holography," Opt. Lett. **26**(20), 1550–1552 (2001).
10. M. Gross, and M. Atlan, "Digital holography with ultimate sensitivity," Opt. Lett. **32**(8), 909–911 (2007).

#111642 - $15.00 USD Received 26 May 2009; revised 24 Jun 2009; accepted 26 Jun 2009; published 25 Sep 2009

11. L. V. Wang, and G. Ku, "Frequency-swept ultrasound-modulated optical tomography of scattering media," Opt. Lett. **23**(12), 975–977 (1998).
12. G. Yao, S. Jiao, and L. V. Wang, "Frequency-swept ultrasound-modulated optical tomography in biological tissue by use of parallel detection," Opt. Lett. **25**(10), 734–736 (2000).
13. B.C. Forget, F. Ramaz, M. Atlan, J. Selb, and A. C. Boccara, "High-contrast fast Fourier transform acousto-optical tomography of phantom tissues with a frequency-chirp modulation of the ultrasound," Appl. Opt. **42**(7), 1379–1383 (2003).
14. M. Gross, P. Goy, B. C. Forget, M. Atlan, F. Ramaz, A. C. Boccara, and A. K. Dunn, "Heterodyne detection of multiply scattered monochromatic light with a multipixel detector," Opt. Lett. **30**(11), 1357–1359 (2005).
15. T. W. Murray, L. Sui, G. Maguluri, R. A. Roy, A. Nieva, F. Blonigen, and C. A. DiMarzio, "Detection of ultrasound-modulated photons in diffuse media using the photorefractive effect," Opt. Lett. **29**(21), 2509–2511 (2004).
16. L. Sui, R. A. Roy, C. A. DiMarzio, and T. W. Murray, "Imaging in diffuse media with pulsed-ultrasound-modulated light and the photorefractive effect," Appl. Opt. **44**(19), 4041–4048 (2005).
17. M. Gross, F. Ramaz, B.C. Forget, M. Atlan, A. C. Boccara, P. Delaye, and G. Roosen, "Theoretical description of the photorefractive detection of the ultrasound modulated photons in scattering media," Opt. Exp. **13**(18), 7097–7112 (2005).
18. F. Ramaz, B. C. Forget, M. Atlan, A. C. Boccara, M. Gross, P. Delaye, and G. Roosen, "Photorefractive detection of tagged photons in ultrasound modulated optical tomography of thick biological tissues," Opt. Exp. **12**(22), 5469–5474 (2004).
19. M. Lesaffre, F. Jean, F. Ramaz, A. C. Boccara, M. Gross, P. Delaye, and G. Roosen, "In situ monitoring of the photorefractive response time in a self-adaptive wavefront holography setup developed for acousto-optic imaging," Opt. Exp. **15**(3), 1030–1042 (2007).
20. M. Gross, M. Lesaffre, F. Ramaz, P. Delaye, G. Roosen, and A. C. Boccara, "Detection of the tagged or untagged photons in acousto-optic imaging of thick highly scattering media by photorefractive adaptive holography," Eur. Phys. J. E **28**(2), 173–182 (2009).
21. Y. Li, H. Zhang, C. Kim, K. H. Wagner, P. Hemmer, and L. V. Wang, "Pulsed ultrasound-modulated optical tomography using spectral-hole burning as a narrowband spectral filter," Appl. Phys. Lett. **93**, 011111 (2008).
22. Y. Li, P. Hemmer, C. Kim, H. Zhang, and L. V. Wang, "Detection of ultrasound-modulated diffuse photons using spectral-hole burning," Opt. Exp. **16**(19), 14862–14874 (2008).
23. M. Hisaka, T. Sugiura, and S. Kawata, "Optical cross-sectional imaging with pulse ultrasound wave assistance," J. Opt. Soc. Am. A **18**(7), 1531–1534 (2001).
24. M. Atlan, B. C.Forget, F. Ramaz, A. C. Boccara, and M. Gross, "Pulsed acousto-optic imaging in dynamic scattering media with heterodyne parallel speckle detection," Opt. Lett. **30**(11), 1360–1362 (2005).
25. C. Kim, R. J. Zemp, and L. V. Wang, "Intense acoustic bursts as a signal-enhancement mechanism in ultrasound-modulated optical tomography," Opt. Lett. **31**(16), 2423–2425 (2006).
26. E. Bossy, L. Sui, T. W. Murray, and R. A. Roy, "Fusion of conventional ultrasound imaging and acousto-optic sensing by use of a standard pulsed-ultrasound scanner," Opt. Lett. **30**(7), 744–746 (2005).
27. X. Xu, H. Zhang, P. Hemmer, D. Qing, C. Kim, and L. V. Wang, "Photorefractive detection of tissue optical and mechanical properties by ultrasound modulated optical tomography," Opt. Lett. **32**(6), 656–658 (2007).
28. G. Rousseau, A. Blouin, and J. P. Monchalin, "Ultrasound-modulated optical imaging using a powerful long pulse laser," Opt. Exp. **16**(17), 12577–12590 (2008).
29. P. Santos, M. Atlan, B. C. Forget, F. Ramaz, A. C. Boccara, and M. Gross, "Acousto-optic imaging with a digital holography scheme: new scheme to obtain axial resolution," Proc. SPIE **5864**, 586401 (2005).
30. T. Y. Chang, A. E. Chiou, and P. Yeh, "Cross-polarization photorefractive two-beam coupling in gallium arsenide," J. Opt. Soc. Am. B **5**(8), 1724–1729 (1988).

## 1. Intoduction

Acousto-optic imaging (AOI) [1, 2, 3] is a technique that couples ultrasounds and light in order to reveal the local optical contrast of absorbing *and/or* scattering objects embedded within thick and highly scattering media, *e.g* human breast tissues. Ultrasonic waves for Medicine (at a few $MHz$) are ballistic and weakly absorbed, and thus give a direct spatial localization of the signal, without solving an inverse diffusion equation. Let us recall that the coupling between an ultrasonic wave at frequency $\omega_{US}$ and a temporally coherent beam (frequency $\omega_L$) generates weak sidebands (so called *tagged-photons* [4]), shifted from the US frequency, *e.g* $(\omega_L \pm \omega_{US})$. This property also known as the acousto-optic effect [3] is due to the US modulation that monitors the phase of the optical wave through a variation of both the refractive index of the medium and the displacement of scatterers at the location of the US beam. The principle of AOI is based

#111642 - $15.00 USD Received 26 May 2009; revised 24 Jun 2009; accepted 26 Jun 2009; published 25 Sep 2009

on the *flux* collection of one of these sidebands: an absorber positioned within the US volume reduces this quantity at the output of the sample, and thus a $3D-scan$ of the US emitter can reveal the local optical properties of the sample.

First experiments used fast mono detectors to record the modulation of the optical signal at the US frequency [1, 2, 3, 5, 6, 7]. But, since the phase of the modulation is different for each grain of speckle, the detector can only process one grain of speckle. To increase the detection of the optical *etendue*, Leveque et al. [4]have developed a camera detection technique that processes many speckles in parallel. This technique has been pulled to the photon shot noise limit by Gross et al. [8] using a holographic heterodyne technique [9] able to detect photons with optimal sensitivity [10]. Since the US attenuation is low in tissues, the tagged photons are generated along the US propagation *z* axis with a nearly constant rate. This means that in a continuous regime of the US, the AO techniques give nearly no information on the location of the embedded objects along the *z* axis. To get such *z* information, Wang et al. [11] have developed an US frequency chirp technique with a single detector, which has been extended to camera detection [12, 13]. Unfortunately, these chirp techniques cannot be used in living tissues, because the phase of light decorrelates very fast in them [5, 14]: the half frequency linewidth of light that travels through 4 cm of living breast tissue is about 1.5 kHz [14]. This phase decorrelation drastically lowers the detection efficiency. Because coherent detection is performed, the detection bandwidth is approximately equal to the camera frame rate. The bandwidth is then much narrower than the width of the scattered photon frequency spectrum, thus most of the tagged photons are undetected. It is still possible to increase the detection bandwidth by using a faster camera, but in such systems this generally means that a smaller number of pixels should be used, and the detection optical *etendue* decreases accordingly.

In order to get a detection bandwidth comparable with the signal bandwidth while keeping a large optical etendue, detection schemes involving photorefractive (PR) crystals have been proposed.

Murray et al. use a PR crystal sensitive @532 nm to select the untagged photons, which are detected by a single avalanche photodiode [15, 16]. In this case, the weight of the tagged photon signal is measured indirectly by using the conservation law of the total number of photons (tagged + untagged) [17]. Ramaz et al. selectively detect either the tagged or the untagged photons [18]. The Ramaz technique is also able to measure in situ the photorefractive writing time ($\tau_{PR}$), which characterizes the detection frequency bandwidth [19]. Photorefractive times $\tau_{PR}$ comparable with the phase decorrelation time ($1/\Delta\nu$) have been reported [20]. Very recently, Li et al. have proposed to detect selectively the *tagged* and *un-tagged* photons with large bandwidth and *etendue*, by using spectral holeburning [21, 22].

In order to get information on the location of the object along the *z* axis, acoustic pulses are used. The method has been extensively used both with single detectors [23, 6], cameras [24, 25], and PR crystals [15, 16, 26, 27, 28]. Nevertheless, reaching a millimetric resolution with US pulses requires a typical duty cycle of 1%, corresponding to the exploration length within the sample ($\sim$ 10 cm) and the desired resolution ($\sim$ 1 mm).

This is problematic regarding the very small quantity of light that emerges from a clinical sample, since weak duty cycle yields low signal and poor Signal-to-Noise Ratio (*SNR*). When US pulses are used with photodiode detection, the *SNR* problem may be enhanced, since fast photodetectors mean larger electronic noise.

In this letter we propose an original technique called Acousto-Optical Coherence Tomography (AOCT), compatible with PR detection of the tagged photons, able to provide *z* resolution with a 100% duty cycle US beam. Since the *z* resolution is not related to the detection of fast optical transients, large area slow photodiode electronic systems, which have great efficiency and low noise, can be used. Obviously, this technique does not allow us yet to match the medical

#111642 - $15.00 USD Received 26 May 2009; revised 24 Jun 2009; accepted 26 Jun 2009; published 25 Sep 2009

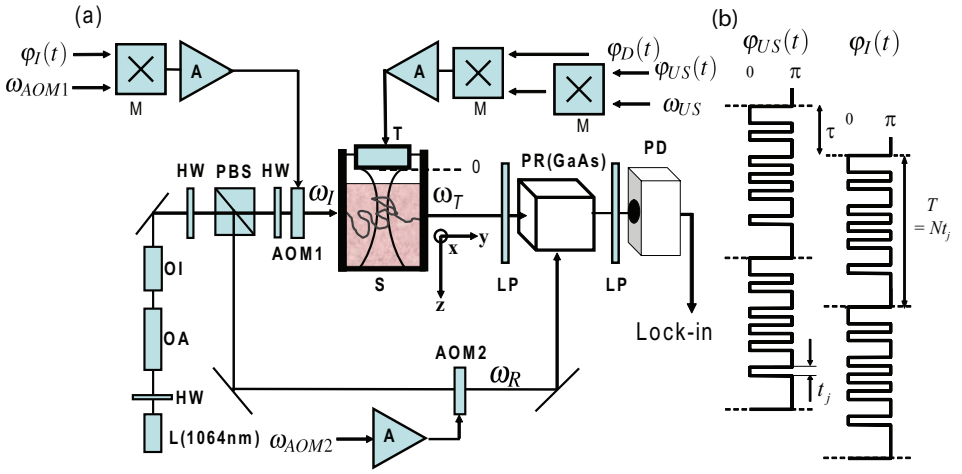


Fig. 1. (a) Experimental setup. L: 1W Nd:YAG laser; OA: 5W Yb-doped optical amplifier; OI: optical Faraday isolator; HW: half-wave plate; AMO1,2: acousto-optic modulator; S: sample; PBS: polarizing beam-splitter; T: acoustic-transducer; M: double balanced mixer; PR: photorefractive GaAs crystal; LP: linear polarizer; PD: $0.3cm^2$ Si photodiode; $\varphi_D$: additional phase modulation for the detection (rectangular shape $(0;\pi)$), at a frequency $\omega_D = 3$kHz, with a 24% duty cycle. (b) Respective phase modulations of the incident beam $\varphi_I$ and the US beam $\varphi_{US}$.

standards, however combining it with pulses [28] could make it possible.

In its principle, the technique is performed by application of a stochastic phase modulation on light and ultrasound. By this way we get a short coherence length US source that explores the sample. A time delay between the US and light modulation enables to select the active zone along the US column where the acousto optic interferometric signal remains coherent in time. Axial resolution can be obtained by this way, as in conventional Optical Coherence Tomography (OCT).

The experimental demonstration of our AOCT technique is performed with a self-adaptive holographic setup including a GaAs PR crystal working @1064*mn* in an anisotropic diffraction configuration [20]. Our observations confirm preliminary results that have been obtained with tagged photons camera detection [29].

## 2. The *z* selection method

In a typical acousto optic imaging experiment (see Fig.1), the incident beam (field $E_I$, frequency $\omega_I$) interacts, within the sample S, with a US beam ($\omega_{US}$), which generates a tagged photon field $E_T$, of frequency:

$$\omega_T = \omega_I + \omega_{US} \tag{1}$$

This field interferes within the PR crystal with a reference field ($E_R$, $\omega_R$), and generates a volume hologram. In order to detect selectively the tagged photons, the illumination and reference beams are shifted in frequency through two acousto optic modulators (AOM1 and AOM2) in order to satisfy

$$\omega_R = \omega_I + \omega_{US} = \omega_T \tag{2}$$

#111642 - $15.00 USD Received 26 May 2009; revised 24 Jun 2009; accepted 26 Jun 2009; published 25 Sep 2009

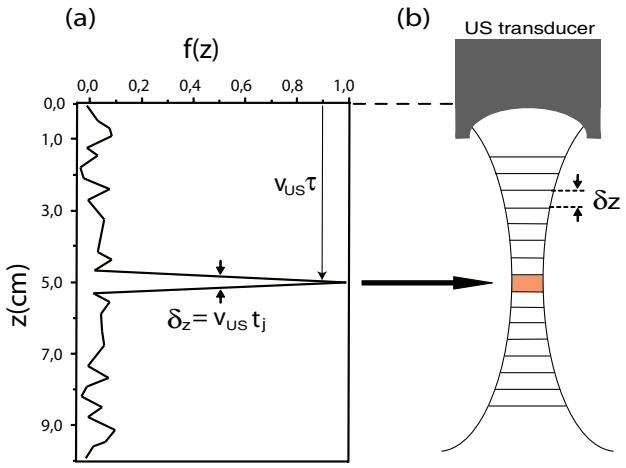


Fig. 2. (a) Numerical simulation of the autocorrelation function $f(z)$ of $e^{j\varphi_T(z)}$ for a US phase modulation sequence with $N = 512$ random $(0,\pi)$ jumps within $T_j = 1$ ms. The typical shape is a triangle of $\delta z = v_{US} t_j \simeq 3$ mm in width at half maximum.(b) Schematic representation of the coherence slice along the US beam.

To get $z$ resolution, the phases $\varphi_{US}$ of the US beam, and $\varphi_I$ of the optical illumination are randomized with the same phase law, but the optical phase is delayed in time by $\tau$:

$$\varphi_I(t+\tau) + \varphi_{US}(t) = 0 \tag{3}$$

Let us introduce the phase $\varphi_T(z)$ of the tagged photons that are generated by the scatterers located within a slice at a coordinate $z = v_{US}\tau$ along the US propagation axis (where $v_{US} \simeq 1500$ m/s is the US velocity) . For this slice , the tagged photons can be detected with full efficiency, since the phase $\varphi_T$ is not randomized with time $t$:

$$\varphi_T(v_{US}\tau) = \varphi_{US} + \varphi_I = 0 \tag{4}$$

Out of the slice $v_{US}\tau$, the phase $\varphi_T(z)$ remains randomized, and the scatterers do not contribute to the average signal. Indeed, the photons outside the coherence volume of extension $v_{US}\tau$ carry a rapid phase modulation with an amplitude of $\pi$, that washes out the hologram they write with the reference beam in the photorefractive crystal. Therefore, only the photons crossing the coherence volume can participate in the writing of the hologram. We must then choose a jump time $t_j$ that is much shorter than the photorefractive response time $\tau_{PR}$ which corresponds to the time required to build a hologram.

Figure 1 (b) illustrates how the phases of the illumination and the US beams are randomized in our experiment. By using two DBM (Double Balanced Mixers ZAD-1H: Mini-Circuits Lab. Inc.), the sine wave signals of frequency $\omega_{AOM1}$ and $\omega_{US}$ are mixed with two correlated random phase signals $e^{j\varphi_I(t)} = \pm 1$ and $e^{j\varphi_{US}(t)} = \pm 1$ that are generated by two 80 MHz arbitrary waveform generators (Agilent 33250A) with a common 10 MHz reference clock. Because of the finite memory of the generators, the phase signals, which make random jumps at time intervals of $t_j$, are periodic (pseudo random) with periodicity $T_j = Nt_j$. Figure 2 shows the autocorrelation function $f(z)$ of the tagged photons phase distribution $e^{j\varphi_T(z)}$ obtained for a typical random sequence having $N = 512$ and $T_j = 1$ ms. The expected resolution is equal to the width $\delta z$ of $f(z)$, which is simply:

$$\delta z = v_{US} t_j \tag{5}$$

#111642 - $15.00 USD Received 26 May 2009; revised 24 Jun 2009; accepted 26 Jun 2009; published 25 Sep 2009

In our experiment, we have $T_j = 1/32$ s and $N = 16384$ yielding $t_j = 1.9\mu$s and therefore $\delta z = 2.85$mm.

## 3. The experimental setup

The experimental setup is presented in Fig.1. It is close to the setup described elsewhere [19, 20]. The master laser L (wavelength $\lambda_L = 1064nm$, 5 W) is single mode (transverse and longitudinal) and vertically polarized. It illuminates the sample with respect to the safety norms @1064*nm* ( e.g power: 0.5 W, area 1 cm$^2$). The acoustic transducer (Panametrics A395S-SU, focal length of 75*mm*) generates a US beam of main frequency $\omega_{US} = 2.3MHz$, with 1.6 MPa at the focal point. The relative power of the reference and illumination beams is adjusted by a half wave plate (HW) followed by a polarizing beam splitter (PBS).

The PR crystal is a bulk GaAs crystal of $1.4 \times 1.6cm^2$. The crystal is oriented into an anisotropic diffraction configuration [30, 28]. The signal beam, and the reference beam, which is vertically polarized, enter on orthogonal faces, respectively $(11\sqrt{2})$ and $(11\overline{\sqrt{2}})$, in order to have a grating vector along $< 001 >$. In such a configuration, the effective electrooptic coefficient is $r_{eff} = r_{41}$.

A polarizer oriented at $\pi/4$ from vertical is positioned after the sample, while a horizontal polarizer is positioned after the crystal. This configuration minimizes the main parasitic light contribution, that corresponds to the scattering of the intense reference by the PR crystal. For the reference beam we use (power 650 mW, area 0.32 cm$^2$) the photorefractive response time is $\tau_{PR} = 3.4$ *ms*.

The signal detection procedure is analogous to our previous works [18, 19, 17]. Here, because of the axial *z* selection procedure, we must consider only the tagged photons that have been created within the *z* selected slice. Thus the field $E_S$ represents only these selected tagged photons. It takes a time equal to $\tau_{PR}$ to the interference term $E_S E_R^*$, where $E_R$ is the reference beam field, to generate a PR hologram. Thus the latter diffracts a component $E_D$:

$$E_D \propto \frac{\langle E_S E_R^* \rangle_{\tau_{PR}}}{|E_S|^2 + |E_R|^2} E_R \tag{6}$$

where $\langle\ \rangle$ represent the time average.

The signal detected on the photodiode is proportional to $E_S E_D^*$. In order to get a time varying signal on the photodiode PD, we apply on the US beam, by using another mixer M, an extra rectangular signal $e^{j\varphi_D} = \pm 1$ at frequency $\omega_D = 3\text{kHz} \gg 1/\tau_{PR}$ with a 24% duty cycle. Thus the time-averaged value of the signal is non-zero. The PD signal is then modulated at $\omega_D$, because $E_S$ is modulated while $\langle E_S \rangle^*$ is not. The photo detector PD is a $0.3cm2$ silicon photodiode (Hamamatsu S2386-8k) connected to a home-made $10M\Omega$ transimpedance amplifier. This amplifier is followed by a AC coupled $100\times$ amplifier that acts as a high-pass frequency filter in order to cancel the *cw* contributions that can saturate the input of the lockin detection (*EG*&*G* Inc. 7210). To optimize *flux* detection without the use of lenses, we have stacked the ensemble (sample+crystal+photodetector) together.

## 4. The experimental results

A first experimental test has been performed with an *Agar+Intralipid*10% phantom of thickness $e = 3cm$ along the illumination direction *y* with a reduced scattering coefficient $\mu_s' =$ 6 cm$^{-1}$@1064*nm*. A black inked absorbing inclusion is embedded within the sample. It is a cylinder of 3 mm in diameter (see insert of Fig.3), and 7 mm in length along the *y* axis which corresponds to the illumination master axis. The US beam is focused within the medium along the *z* axis in a plane located at $1.5cm$ from the input.

#111642 - $15.00 USD Received 26 May 2009; revised 24 Jun 2009; accepted 26 Jun 2009; published 25 Sep 2009

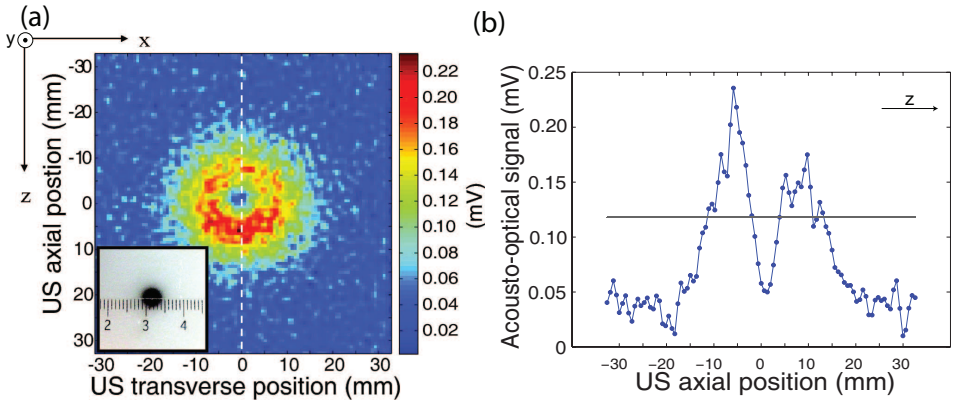


Fig. 3. (a) Acousto-optic 2D-profile of an optical absorber ($x \times y \times z = 3 \times 7 \times 3$ mm$^3$) embedded within a scattering gel ($\mu_s^{'} = 6$ cm$^{-1}$, thickness = 3 cm) performed with a random phase sequence of $z = 2.85$ mm axial resolution . Note that the 2D profile $(x,y)$ is orthogonal to the longitudinal axis of the light diffusion "banana", and to the absorbing sample cylinder axis ($y$). As a consequence, the image is nearly symmetric by rotation. (b) Cut along the white dashed line axis of Fig.3a.

The *xz* image shown on Fig.3 is obtained by scanning both the position of the US transducer (along the US transverse *x* axis), and the delay $\tau$ (along the US longitudinal *z* axis). Each pixel is obtained with an integration time of 400 ms using a lock-in time constant $T_{lock-in} = 100$ ms. The $100 \times 100$ pixels zone that is displayed corresponds to a surface of $6.5 \times 6.5$ cm$^2$ within the sample. The maximum spatial frequency of the raw data is thus $k_{max} = 1/0.65 mm^{-1}$. A spatial filter, which consists in a crop within the spatial Fourier plane with a cut-off frequency $k_c = 1 mm^{-1}$, is applied to improve SNR. We expect indeed no information from greater spatial frequencies since the US transverse resolution is about $2mm$ on both sides of the US focal spot.

One can see, on Fig.3 a nearly circular zone of 25 mm in diameter corresponding to the lateral extent of the scattering banana. In the center of the zone, one can see a narrow (3-4 mm) circular dip, which corresponds to the cylindrical absorbing inclusion. To make a more quantitative analysis of the image of Fig.3, we have performed a vertical cut along the *z* direction in the center of the dip (vertical dashed white line). Figure 3 shows the tagged photon signal along the cut. The absorbing inclusion causes a drop in the signal at $z = 0$ mm to a level close to the background level. This result proves that the *z* resolution we get is better than the diameter (3 mm) of the absorbing zone. This observation is in agreement with the expected resolution($\delta z =$ 2.85 mm).

We have performed a second experimental test with a phantom consisting of 2 inclusions located on the vertical *z* axis (see insert of Fig.4). The sample thickness is 2 cm with $\mu_s' = 10$ cm$^{-1}$@$1064nm$. Inclusions are also cylindrical and are 3 mm in diameter,4.5 mm in length and have a 2 mm separation along *z*. The $60 \times 60$ pixels image on Fig.4 corresponds to $3 \times 2.6$ cm$^2$ on the sample in the *x* and *z* direction respectively with a lock-in time constant $T_{lock-in} = 500$ ms . The random phase sequence ($\delta z = 2.85$ mm), and the other parameters are the same as for the first sample. Figure 4 illustrates the resolution of our random phase technique, since the two inclusions can be distinguished.

In order to remain in conformity with safety norms , one can change the location of the US focus point in the transverse directions *x* and *y*, when applying successive 1.6 MPa, $T_j = 1$ ms random phase sequences. By this way, the medium may relax regarding to the US absorption.

#111642 - $15.00 USD Received 26 May 2009; revised 24 Jun 2009; accepted 26 Jun 2009; published 25 Sep 2009

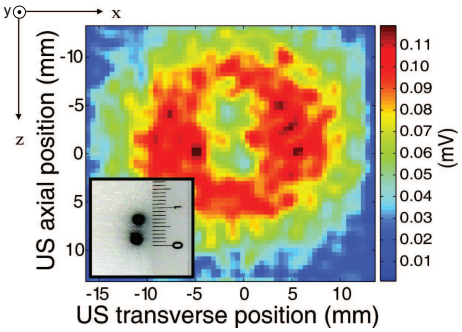


Fig. 4. Acousto-optic $60 \times 60$ image of 2 optical absorber of diameter 3 mm separated by 2 mm along $z$ embedded within a scattering gel ($\mu_s^{'} = 10cm^{-1}$, thickness = 2 cm) performed with a random phase sequence of $z = 3$ mm axial resolution.

## 5. Conclusion

We have proposed and experimentally demonstrated a new technique able to provide axial $z$ resolution in acousto optic imaging with photorefractive detection of the tagged photons. Our AOCT technique is a low coherence imaging technique like OCT (Optical Coherence Tomography) that involves "low coherence acousto optic sources", i.e. an optical and an US source, which are both incoherent in time, but fully correlated together.

This work has been supported under a grant from the *Canceropôle Ile-de-France*.

#111642 - $15.00 USD Received 26 May 2009; revised 24 Jun 2009; accepted 26 Jun 2009; published 25 Sep 2009